



NONLINEAR FLAME DYNAMICS AND MODE TRIGGERING IN A MULTIPLE FLAME COMBUSTOR

Frédéric Boudy*, Daniel Durox, Thierry Schuller and Sébastien Candel†

Laboratoire EM2C, CNRS and Ecole Centrale Paris
Grande Voie des Vignes, 92290 Châtenay-Malabry, France

† also with Institut Universitaire de France

* Corresponding author: frederic.boudy@em2c.ecp.fr

A Flame Describing Function (FDF) framework recently developed to assess the stability of an unconfined premixed combustor is here used to examine the dynamics of a generic system including a feeding manifold a multipoint injector and a flame tube confining the combustion zone. The feeding manifold has a variable length which is used as a bifurcation parameter in the instability analysis of this system. Self-sustained oscillations are characterized at their limit cycle for different sizes of the feeding manifold. Using the FDF framework, frequencies and limit cycles are predicted and compared with experimental values measured on the combustor. It is shown that limit cycles are well predicted by taking into account the nonlinear response of the flame. This is also used to explain nonlinear mode triggering observed in certain ranges of the feeding manifold length.

1 Introduction

The possibility of a resonant coupling between combustion and acoustics was recognized more than a hundred years ago [1]. The problem has since been encountered in a variety of combustion applications leading to numerous investigations of these instabilities (see for example classical monographies [2, 3] and [4–8] for more recent reviews). Much progress has been made in the understanding and control of combustion dynamics but research is still needed to develop predictive tools and design systems with augmented stability margins. One difficult aspect is to account for the nonlinear flame dynamics which is manifested in practice.

In many studies the flame response to incoming perturbations is represented in a linear fashion. This is well illustrated in the sensitive time lag model [2] where this response is formulated in terms of an interaction index n and a time delay τ . This has been generalized by introducing the Flame Transfer Function (FTF), which is now commonly used to predict stability maps of laminar or turbulent configurations [9–12]. The FTF accounts for the frequency dependent response which approaches a quasi-steady behavior at low frequencies and filters out higher frequencies. The FTF relates heat release rate fluctuations to incident flow perturbations and is easily included in linear stability analysis to estimate instability ranges of combustion systems [10, 12–14].

It is however known, that many features observed during unstable oscillations cannot be anticipated from the FTF. This is illustrated in [12] where the linear stability analysis provides resonant frequencies which are close to, but do not quite match, experimentally observed frequencies. It is shown that the flame shape is strongly modified when perturbation amplitudes increase [15, 16]. Saturation effects have been identified for many flame geometries and shown to occur through different mechanisms and it is now clear that the input level must be considered to represent the flame response to incoming flow perturbations [7, 15, 17–20]. This has already been shown for swirled flames featuring saturation phenomena and nonlinear dynamics [21]. Besides, many studies reveals that the flame front geometry

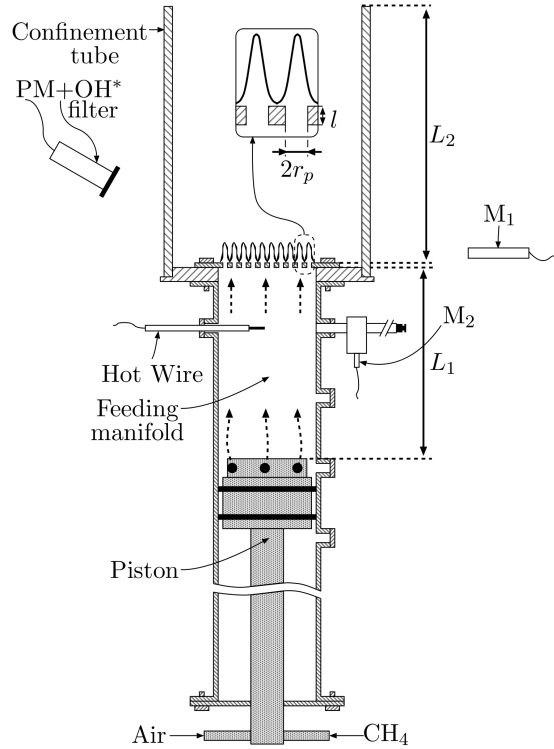


Figure 1: Experimental setup used to characterize self-sustained instabilities.

plays a major role on the nonlinear response between the heat release rate fluctuations and the perturbations [14–16, 20]. To improve the quality of the stability maps, a nonlinear analysis is clearly needed.

It is possible to include saturation as illustrated in an analysis of the stability of a ducted “V”-flame [17] by using different expressions for the FTF depending on the amplitude level of velocity fluctuation at the flame anchor point. When the level is below a certain threshold an analytical model for the FTF is used. When the threshold is exceeded heat release rate fluctuations are assumed to saturate to a constant value. This can be generalized by making use of the Flame Describing Function (FDF) framework devised more recently by [22]. The FDF, formed by a family of transfer functions corresponding to a range of input levels, depends on frequency and amplitude. When this is used in combination with a linear acoustics description of the other elements in the system, one can obtain a nonlinear dispersion relation which yields amplitude dependent growth rates and resonant frequencies. Application to an unconfined multiple injection configuration provides amplitude levels at the limit cycles, and allows predictions of mode switching, triggering and hysteresis [22].

The present study extends this development by considering a multipoint injection combustor where a collection of laminar conical flames are anchored on a perforated plate placed in a flame tube. The system presented in section 2 has a generic geometry which typifies that of many practical devices. The FDF framework is applied to this configuration to validate the methodology with respect to experimental data (sections 3 and 4). Frequency shifting during transients, instability triggering, hysteresis and mode switching phenomena are specifically considered (section 5). These features which could not be anticipated from linear stability analysis are here obtained from the FDF framework.

2 Experimental setup and combustion regimes

The experimental setup is sketched in Fig. 1. The three main elements of the burner are the feeding manifold, a perforated plate which delivers the premixed streams and anchors the flames and the quartz

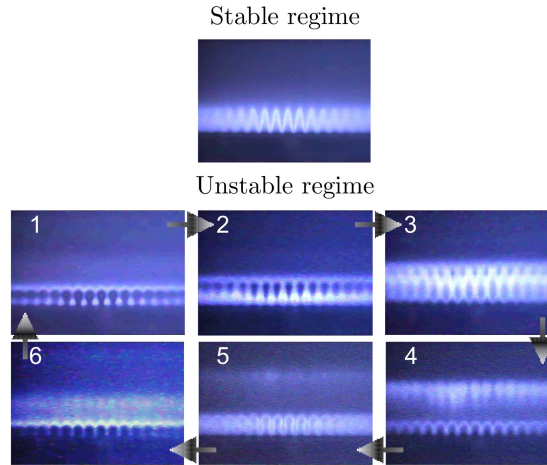


Figure 2: Stable and unstable combustion regimes at 750 Hz for an equivalence ratio $\phi=1.03$.

confinement tube. The combustion zone is confined by this quartz tube. The reactants are premixed in the piston before they are injected into the enclosing manifold. The piston also allows changes in the length of the feeding manifold. The perforated plate, which is confined within a quartz tube at the top of the feeding manifold, anchors an ensemble of small laminar conical flames. It has a thickness of $l=3$ mm and a diameter of $2R=70$ mm. It is made of stainless steel and comprises $N=420$ holes of diameter $2r_p=2$ mm placed on a 3 mm square mesh, resulting in a global porosity $\mathcal{P} = N\pi r_p^2/\pi R^2$ of 0.34. Four quantities are measured in this experiment. The fluid velocity in the feeding manifold is determined with a hot wire probe located at a distance of 3 cm below the perforated plate. A photomultiplier equipped with an OH^* filter ($\lambda=308$ nm) views the flames from outside the confinement tube and provides a signal which is nearly proportional to the heat release rate [23, 24]. Pressure fluctuations are measured inside the feeding manifold with the microphone M_2 placed in a waveguide in front of the hot wire and another microphone M_1 outside the confinement tube 24.5 cm away from the burner axis detects the radiated sound pressure level. The length of the feeding manifold, as measured between the upstream side of the perforated plate and the head of the piston, can be varied in discrete steps all the way from $L_1=0.15$ m to 0.54 m. The piston head is designed to offer a quasi-perfect reflecting boundary for acoustic waves. A confinement tube of $L_2=0.1$ m enclose the combustion zone. The flow rate of the methane/air mixture is $\dot{m}=4.71 \times 10^{-3}$ kg/s with an equivalence ratio $\phi=1.03$, providing a thermal power of 13.3 kW.

Combustion is first initiated with the piston placed at $L_1 = 0.15$ m from the perforated plate and the signals from the different sensors are recorded at this location. The piston is then moved to a new location and experiments are repeated for a larger manifold size by increments of one centimeter until $L_1=0.54$ m is reached. In a second set of experiments, combustion is initiated for $L_1 = 0.54$ m and experiments are carried out by moving the piston in the reverse direction. Under stable operation, flames have a conical steady shape (top of Fig. 2). Under unstable conditions, the flames move in a synchronized fashion with a periodic shedding and subsequent collapse of small pockets of fresh gases formed (bottom of Fig. 2). This yields a noise level exceeding 110 dB (ref 2×10^{-5} Pa) at microphone M_1 . Oscillation amplitudes and frequencies can be extracted from the different signals and are analyzed as a function of the feeding manifold cavity size L_1 and the direction of the piston motion. Another set of experiments is conducted to get the response of the flame ensemble to velocity fluctuations and to determine the FDF [22]. Heat release rate fluctuations are determined with fluctuations of the OH^* radical emission recorded by a photomultiplier (PM). Velocity fluctuations used to determine the FDF are obtained from LDV (Laser Doppler Velocimetry) measurements inside one flame 0.7 mm above the hole.

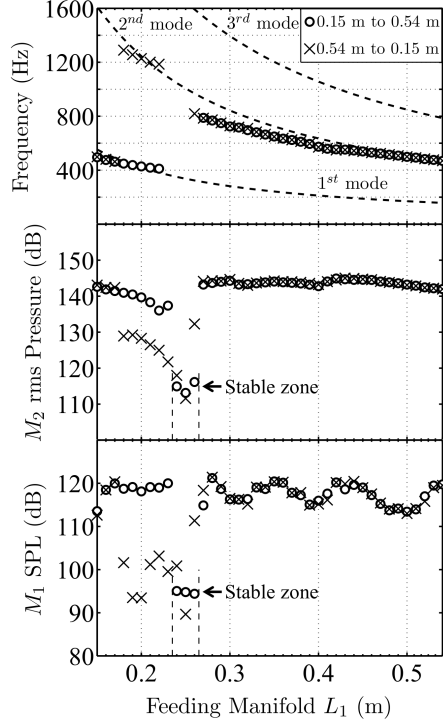


Figure 3: Frequency and pressure level evolution with the $L_2=0.1$ m confinement tube, swept from 0.15 m to 0.54 m (o) and from 0.54 m to 0.15 m (x) of feeding manifold. The acoustic eigenmodes without combustion are plotted with dashed lines.

3 Experimental results

Figure 3 illustrates the evolution of frequency and pressure for different lengths of feeding manifold (L_1) and a confinement tube of $L_2=0.1$ m. The dashed lines represent the acoustic eigenmodes evolution for a variable feeding manifold length L_1 . The system features self-sustained oscillations for all cavity lengths L_1 except between 0.24 and 0.26 m where combustion is stable. Results obtained by increasing the manifold length indicate that the oscillation frequency lies around the first acoustic mode when L_1 ranges from 0.15 m to 0.23 m, then the oscillation vanishes in the band $L_1=0.24$ m to 0.26 m. The peak frequency then evolves around the second acoustic mode for longer cavity depths ($L_1=0.27$ m to 0.54 m). The corresponding pressure level at M_2 lies around 142 dB when the system is unstable and is roughly independent of L_1 . When the piston is moved in the reverse direction, the peak oscillation frequency remains locked to the second mode from $L_1=0.54$ m to 0.26 m and the oscillation level is about equal to that found in the previous case. The oscillation then vanishes in the stable band, but from $L_1=0.22$ m to 0.18 m the frequency is still locked on the second acoustic mode with a moderate amplitude level. The peak frequency finally switches to the first acoustic mode for the shortest cavity sizes $L_1=0.17$ m to 0.15 m with an oscillation level equal to that found in the first set of experiments. The system clearly features an hysteresis for the range of feeding manifold lengths comprised between 0.18 and 0.22 m where the oscillation frequency and level depend on the history of the piston motion. Such features cannot be anticipated from a linear stability analysis and they constitute a good benchmark for validation of the FDF nonlinear methodology.

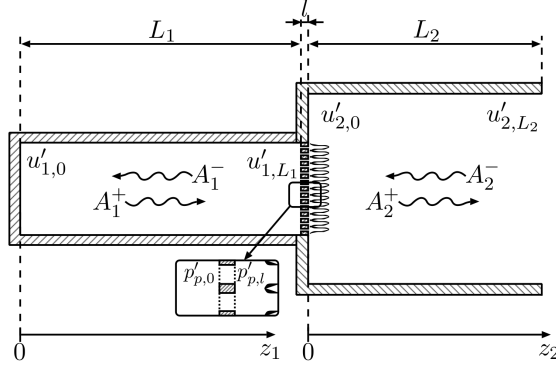


Figure 4: Burner and symbol convention used for the analytical model.

4 Nonlinear analysis

A nonlinear stability analysis based on the FDF is now carried out. In the following analysis, fluctuating quantities are written as a sum of a mean quantity and a fluctuation : $a = \bar{a} + a'$. The analysis is performed in the frequency domain and each fluctuating quantity takes the form : $a' = |a'|e^{-i\omega t}$ where $\omega = \omega_r + i\omega_i$, ω_r corresponding to the angular frequency ($2\pi f$) and ω_i denoting the growth rate. A perturbation grows for positive values of ω_i while it decays for negative ones. The analytical development follows that devised previously [25]. Given the low unstable frequencies observed in the experiments, the wavelengths are long compared to the dimensions of the system and one may safely consider that acoustic propagation only involves longitudinal waves. The flame region is also very small compared to the wavelength and one may consider that it is compact. The different elements of the system are modeled with an acoustic network. The influence of the flames is taken into account in the matching condition between the feeding manifold and the confinement tube through the expansion of gases. This method is often used to analyze thermo-acoustic coupling phenomena (see for example [11, 26–28]). The burner is modeled as illustrated in Fig. 4. In each tube section, temperature, density, velocity and pressure are all subscripted with their respective numbers and mean quantities (\bar{T} , $\bar{\rho}$) are considered uniform. The pressure and the velocity fluctuations are written as follows for the n^{th} tube :

$$u'_{n,z_n} = \frac{1}{\rho_n c_n} \left(A_n^+ e^{ik_n z_n} - A_n^- e^{-ik_n z_n} \right) \quad (1)$$

$$p'_{n,z_n} = A_n^+ e^{ik_n z_n} + A_n^- e^{-ik_n z_n}$$

where z_n stands for the position, k_n the wave number ($k_n = \omega/c_n$) and c_n the speed of sound which differs in the pre-mixer $c_1=340$ m/s and the flame tube $c_2=850$ m/s. These relations are completed by matching and boundary conditions. The head of the piston offers a quasi-perfect reflecting boundary condition which gives $u'_{1,0} = 0$. At the combustor outlet the pressure fluctuation vanishes and yields $p'_{2,L_2} = 0$. In this model, no end correction is taken into account. This would be easy to include as all it does is to augment the length of the confinement tube by a factor of 0.85 times the radius. The perforated plate is considered with bulk oscillations of velocity in the apertures. Based on Melling's work [29], Noiray et al. [22] used a relation that links the pressure between the upstream and downstream sides of the perforated plate :

$$p'_{p,l} - p'_{p,0} = i\omega\rho_1 l \left(1 + \frac{l_v}{r_p} (1+i) \right) u'_p \quad (2)$$

where $l_v = (2\nu/\omega)^{1/2}$ stands for the viscous acoustic boundary layer thickness and ν the kinematic viscosity. Each side of the perforated plate is linked with the upstream or the downstream cavity where the

following relations are satisfied :

$$p'_{p,0} = p'_{1,L_1}, \quad p'_{p,l} = p'_{2,0}, \quad S_1 u'_{1,L_1} = NS_p u'_p \quad (3)$$

In these expressions S_1 is the surface area of the feeding manifold section, S_p the surface area of one aperture and N the number of holes. Combining Eq. (2) and Eq. (3) it is possible to find the acoustic pressure jump condition between the upstream and downstream cavities :

$$p'_{2,0} - p'_{1,L_1} = i \omega \rho_1 l \left(1 + \frac{l_v}{r_p} (1 + i) \right) \frac{u'_{1,L_1}}{\mathcal{F}} \quad (4)$$

As the perforated plate is thin with a high porosity, one expects that its influence on the acoustic field will be weak. The acoustic volume flow rate experiences a jump through the flame region :

$$S_2 u'_{2,0} - NS_p u'_p = \frac{\gamma - 1}{\rho_1 c_1^2} \dot{Q}' \quad (5)$$

where S_2 represents the confinement section surface area, γ is the heat capacity ratio and \dot{Q}' the heat release rate fluctuation. The right hand side term of Eq. (5) can be expressed by taking into account the response of the flame to velocity fluctuations with a Flame Describing Function (FDF). This quantity is obtained with a setup described in Durox et al. [15]. The conical flames are subjected to harmonic oscillation of increasing fluctuation levels up to 51 % for a range of frequencies up to 1600 Hz. FDF measurements are plotted in Fig. 5 in terms of gain G and phase φ defined as :

$$\mathcal{F}(\omega_r, |u'_p|) = \frac{\dot{Q}' / \bar{Q}}{u'_p / \bar{u}_p} = G(\omega_r, |u'_p|) e^{i\varphi(\omega_r, |u'_p|)} \quad (6)$$

where \bar{Q} stands for the mean value of the heat release rate fluctuation and \bar{u}_p the mean value of the velocity in one hole. The FDF depends on both the frequency ω_r and the fluctuation amplitude u'_p as shown in Fig. 5. When the amplitude increases, the gain G drops and the phase φ evolution shifts confirming the nonlinear behavior of the flame. This is the key point of the nonlinear stability analysis. As shown in this figure, the FDF data are limited by the lack of efficiency from the loudspeaker at high frequency and amplitude. The forcing root mean square velocity level u'_{rms} is determined by a Fourier transform and U_{bulk} stands for the mean value of the velocity profile measured 0.7 mm above one hole by means of LDV. It is equal to $U_{bulk} = 3.1 \text{ m.s}^{-1}$. The normalized ratio between the fluctuation of OH^* radical light intensity and the velocity yields the gain G and the phase φ of the flame response. The flame acts as a low pass filter with a significant overshoot for higher frequencies and low fluctuation amplitudes. This behavior is also noted by other authors [15, 30, 31]. The phase evolves in a quasi linear fashion with the frequency and is sensitive to the fluctuation level. With the aim of using these measures for stability analysis, data are interpolated and extrapolated in missing areas. Considering the right hand side of Eq. (5) and the FDF Eq. (6), one can write :

$$\frac{\gamma - 1}{\rho_1 c_1^2} \dot{Q}' = \frac{\gamma - 1}{\rho_1 c_1^2} \frac{\dot{Q}' / \bar{Q}}{u'_p / \bar{u}_p} \frac{u'_p / \bar{u}_p}{1 / \bar{Q}} \quad (7)$$

In the present study, air and methane are considered to be ideal gases yielding, $c_1 = \sqrt{\gamma r T_1}$, $c_p = \gamma r / (\gamma - 1)$, $\bar{Q} = \dot{m} c_p (T_f - T_1)$, $\dot{m} = \rho_1 NS_p \bar{u}_p$, where r is the gas constant of the mixture, \dot{m} the mixture mass flow rate in one hole, c_p the specific heat at constant pressure, γ the heat capacity ratio and T_f the adiabatic flame temperature. Combining Eqs. (5) to (7), the velocity relation of Eq. (3) and the ideal gas relations, one obtains an expression for the acoustic volume flow rate jump condition across the flame sheet de-

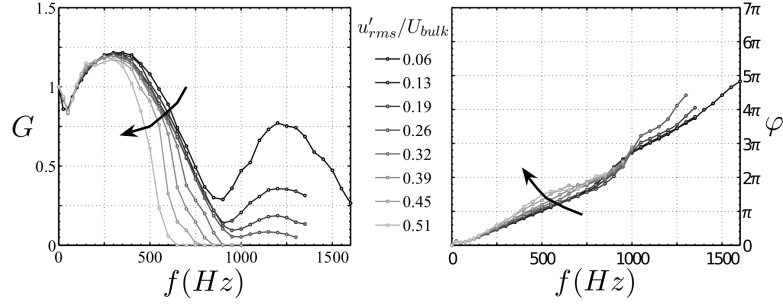


Figure 5: Experimental measurements of the Gain G and Phase φ of the FDE u'_{rms} corresponds to the rms value of the fluctuation amplitude and U_{bulk} the mean flow velocity within one hole.

pending on the FDF :

$$S_2 u'_{2,0} - S_1 u'_{1,L_1} = G e^{i\varphi} S_1 \left(\frac{T_f}{T_1} - 1 \right) u'_{1,L_1} \quad (8)$$

The preceding set of equations can be used to obtain the following linear system :

$$\begin{pmatrix} 1 & -1 & 0 & 0 \\ 0 & 0 & e^{ik_2 L_2} & e^{-ik_2 L_2} \\ \mathcal{A}_1 e^{ik_1 L_1} & \mathcal{A}_2 e^{-ik_1 L_1} & -1 & -1 \\ \mathcal{B} e^{ik_1 L_1} & -\mathcal{B} e^{-ik_1 L_1} & -1 & 1 \end{pmatrix} \begin{pmatrix} A_1^+ \\ A_1^- \\ A_2^+ \\ A_2^- \end{pmatrix} = 0 \quad (9)$$

where the complex coefficients \mathcal{A}_1 , \mathcal{A}_2 and \mathcal{B} correspond to :

$$\mathcal{A}_1 = 1 + \frac{i\omega l}{\mathcal{P}c_1} \left[1 + \frac{l_v}{r_p} (1+i) \right], \quad \mathcal{A}_2 = 1 - \frac{i\omega l}{\mathcal{P}c_1} \left[1 + \frac{l_v}{r_p} (1+i) \right],$$

$$\mathcal{B} = \frac{S_1 \rho_2 c_2}{S_2 \rho_1 c_1} \left[1 + \left(\frac{T_f}{T_1} - 1 \right) G e^{i\varphi} \right]$$

The determinant of this system must equal zero to obtain non-trivial solutions. This condition provides the dispersion relation describing the dynamics of the system :

$$\frac{S_1 \rho_2 c_2}{S_2 \rho_1 c_1} \left[1 + \left(\frac{T_f}{T_1} - 1 \right) G e^{i\varphi} \right] \sin(k_1 L_1) \sin(k_2 L_2)$$

$$- \cos(k_1 L_1) \cos(k_2 L_2) + \frac{\omega l}{\mathcal{P}c_1} \left[1 + \frac{l_v}{r_p} (1+i) \right] \quad (10)$$

$$\cos(k_2 L_2) \sin(k_1 L_1) = 0$$

One then has to find the complex roots $\omega = \omega_r + i\omega_i$ of this relation yielding oscillation frequencies $f = \omega_r/2\pi$ and growth rates ω_i of perturbations as a function of the perturbation amplitude u'_{rms}/U_{bulk} .

5 Theoretical and experimental comparison

The nonlinear analysis described in the previous section is now used to investigate the stability of the system. It is interesting to compare the experimental results from the self-sustained instabilities described in section 3 with the theoretical predictions of the oscillation frequencies and amplitudes at the

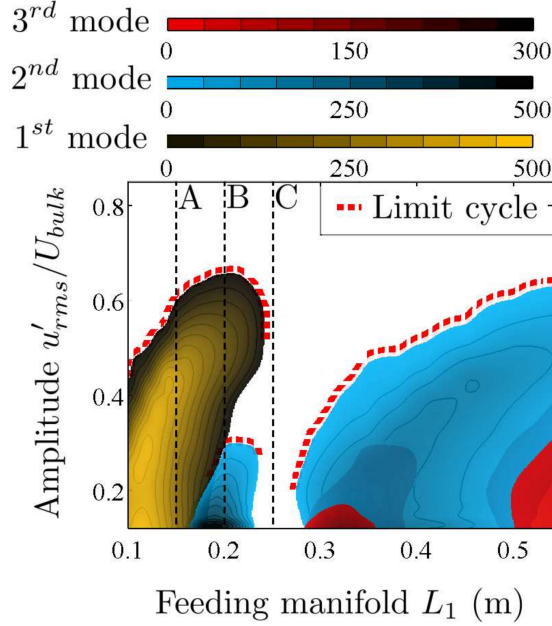


Figure 6: Positive values of the growth rate (in s^{-1}) for a $L_2=0.1$ m flame tube as function of the length L_1 of the feeding manifold and the rate of fluctuation amplitude u'_{rms}/U_{bulk} .

limit cycle. Therefore, the FDF is used to calculate roots of the dispersion relation (10) for each driving amplitude. This yields ω_r and ω_i couples for each burner geometry and driving amplitude. For the different lengths of feeding manifold and the $L_2=0.1$ m confinement tube, calculations give the growth rate evolutions of the three first oscillation modes. Results are displayed in Fig. 6. This figure represents positive values of growth rate. Negative ones correspond to the white zone. Each color is dedicated to an oscillation mode; the first mode is drawn in yellow, the second in blue, and the third in red. Red dashed lines indicate the limit cycle corresponding to vanishing values of the growth rate. (One should in fact consider that the limit cycle is obtained when the growth rate equals the damping rate in the system but in the present experiment, this damping rate is small and it is admissible to just look for locus corresponding to a vanishing growth rate).

From the different growth rate trajectories, it is possible to find, for each geometry, the evolution of the oscillation frequency of an instability up to the limit cycle. As presented in Fig. 6, the growth rates reveal three types of evolution. The first type of trajectory (for example dashed line “A” $L_1=0.15$ m) is positive for a small level of perturbation ($u'_{rms}/U_{bulk}=0.1$) and vanishes for a finite amplitude ($u'_{rms}/U_{bulk}=0.6$), and, as such, defines the limit cycle of the system. In this case, the system is linearly unstable. For the second type (for example dashed line “B” $L_1=0.2$ m), the growth rate of the first mode (yellow zone) is negative for small perturbation amplitudes but becomes positive at an amplitude of $u'_{rms}/U_{bulk}=0.3$ and finally vanishes for a higher amplitude ($u'_{rms}/U_{bulk}=0.65$). This yields a limit cycle that can be triggered by a finite level of perturbation. Indeed, a small level of perturbation cannot create an instability whereas a high oscillation level can. These limit cycles are nonlinearly unstable and linearly stable. For this length, the second mode (blue zone) depicts a first type trajectory as described herein. The saturation level of this mode, around $u'_{rms}/U_{bulk}=0.3$, is able to trigger the nonlinearly unstable first mode. This case is exemplified in Fig. 7. Combustion is initiated in the stable zone and the piston is retracted until reaching $L_1=0.18$ m. The system oscillates around the second mode at $f=1290$ Hz. At $t=0.08$ s an artificial perturbation is created by blowing on the flame and the instability switches to the first mode at $f=449$ Hz. It is worth noting that the experiment has been carried out for a feeding manifold length $L_1=0.18$ m while the case presented in Fig. 6 corresponds to $L_1=0.2$ m. This small discrepancy is due to the accuracy of the theoretical prediction. The last type of trajectory (for example

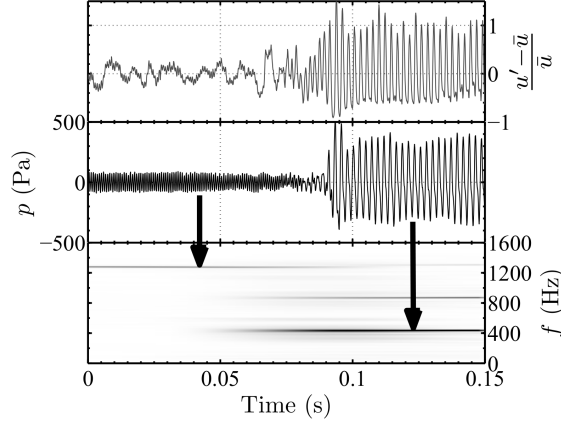


Figure 7: Nonlinear mode triggering for a feeding manifold length $L_1=0.18$ m.

dashed line “C” $L_1=0.25$ m) yields negative values of growth rate for all perturbation levels. In this case, the system is unconditionally stable. Moreover, it can be deemed as both linearly and nonlinearly stable. In summary, it is found that the calculations show three types of growth rate evolution. By analyzing the growth rate for each length of feeding manifold L_1 it is possible to find the limit cycle obtained when $\omega_i=0$ and extract at the same time the oscillation frequency using the angular frequency ω_r . The limit cycle is reached when the growth rate is equal to zero. The acoustic damping δ is not taken into account in these calculations. For systems featuring large damping, limit cycles are reached when $\omega_i - \delta=0$. In the present case, the influence of δ is weak because growth rates take high values typically about 500 s^{-1} whereas δ in this system was estimated to be around 10 to 50 s^{-1} and does not significantly influence the results.

Figure 8 displays the evolution of the predicted oscillation frequencies and the experimental measurements. In these figures, the acoustic eigenmodes, without flame ($G=0$ in the dispersion relation), are drawn as thin dashed lines. The frequencies predicted at the limit cycle using the nonlinear analysis are represented by bold lines and the experimental measurements are plotted as diamond signs. For each length of feeding manifold, (L_1), the frequency is extracted from the oscillations of the pressure signal (M_2). As presented in Fig. 3, there are two types of frequency evolutions. When the manifold length is increased (min to max) (Fig. 8a), the oscillation frequency evolves around the first eigenmode with a change around the second eigenmode after the stable zone between $L_1=0.24$ m and 0.26 m. In the reverse movement (max to min) (Fig. 8b), the frequency lies close to the second eigenmode until it becomes stable at $L_1=0.26$ m, but resumes around the second eigenmode for $L_1=0.23$ m to 0.18 m before it finally switches to the first mode for the last three lengths $L_1=0.17$ m to 0.15 m. This behavior, typical of hysteresis, is well described by the growth rate analysis (see Fig. 6). When the piston is moved in the reverse direction (L_1 decreasing), the oscillation vanishes for three lengths of feeding manifold $L_1=0.26$, 0.25 and 0.24 m. After the stable zone, linearly unstable trajectories for the second mode yield a weak limit cycle between $L_1=0.23$ m and 0.18 m (blue zone). For shorter lengths $L_1 < 0.18$ m, the system is unstable on the first mode (yellow zone) as presented in Fig. 8b. At the beginning, when the manifold cavity was increased from $L_1=0.15$ m to 0.54 m, the system oscillates at high amplitudes for the first lengths $L_1=0.15$ m to 0.17 m. In this case, the instability stays on the first mode even if the growth rate trajectories of this mode become nonlinearly unstable between $L_1=0.18$ m and 0.23 m. The nonlinear perturbation, needed to trigger the first mode, comes from the high oscillation amplitude reached at the previous length. The origin of this hysteresis is linked to the nonlinear behavior of the flame. Indeed, it is possible to predict the hysteresis by analyzing the FDF phase at the acoustic eigenmodes frequencies around the stable zone. If the phase of the FDF is comprised between π and 2π modulo 2π , the instability may develop [25, 32]. When the instability evolves on the first mode at high amplitude (increasing L_1) the phase lies in the right band between π and 2π (see Fig. 5) at $L_1=0.23$ m where $f=400$ Hz whereas

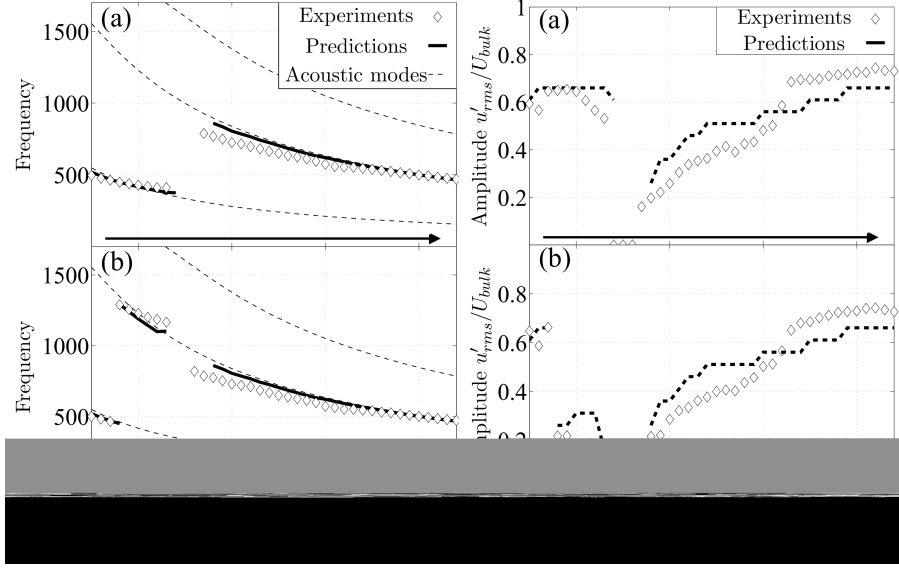


Figure 8: Experimental and predicted oscillation frequencies and amplitudes of self-sustained instabilities for the $L_2=0.1$ m confinement tube for increasing (a) and decreasing (b) length L_1 of the feeding manifold.

this is not the case for the second mode $f=1100$ Hz. When the cavity length L_1 decreases, as the system leaves the stable zone at $L_1=0.23$ m, the phase for low oscillation amplitude lies in the right band for the high frequency $f=1100$ Hz of the second mode. This is the reason why the instability takes on second mode frequency values.

One advantage of the FDF methodology, is that, in addition to providing the limit cycle frequency, the growth rate analysis also predicts the amplitude. For each length of feeding manifold L_1 , it is possible to find the oscillation amplitude when the instability oscillation is established. These results are presented in Fig. 8. The predictions are plotted as dashed lines and the experimental values, obtained by the hot wire probe, appear as diamond signs. Fig. 8a represents the evolution of the amplitude when L_1 is increased. The oscillation evolves at high amplitude for L_1 comprised between 0.15 m and 0.23 m. After the stable zone $L_1=0.24, 0.25$ and 0.26 m, the oscillation grows from a level around 0.19 to 0.7 for longer feeding manifold lengths. By decreasing L_1 , the oscillation evolves in the same way until the stable zone at $L_1=0.26, 0.25$ and 0.24 m. Then, the amplitude switches to a very low level around 0.1, or nearly close to zero for the hot wire values at $L_1=0.23$ m and 0.22 m. After $L_1=0.18$ m, the level increases abruptly to 0.7. The dashed line, which represents the results of calculations, is in good agreement with the levels measured in the experiments.

6 Conclusions

This work presents results of calculations of limit cycles based on the Flame Describing Function (FDF) framework for combustion instability analysis. The system studied herein is close to a real configuration in the sense that it features a feeding manifold that is used to feed a multipoint injector and features a combustion region in a confined environment. The FDF, determined experimentally, exhibits nonlinearities of the flame response. This is used to derive a nonlinear dispersion relation providing predictions of the stable or unstable behavior of the combustor as a function of amplitude. Comparison with systematic experiments were carried out by changing the feeding manifold length. The FDF analysis provides a suitable account of limit cycle amplitudes, hysteresis and mode switching observed in practice. Finally, it should be noted that linear analysis cannot provide reliable stability ranges of a system, because nonlinear triggering is possible in which a high amplitude disturbance exceeding a

threshold may induce self sustained oscillations. This phenomenon is well retrieved from the growth rate trajectories determined from the FDF framework.

Acknowledgment

The research leading to these results has received funding from the European Community's Seventh Framework Programme (FP7/2007-2013) under Grant Agreement #ACP8-GA-2009-234009. This is part of the 4-year KIAI project started in May 2009, which is a European initiative financed under the FP7 and addresses innovative solutions for the development of new combustors in aero-engines. It aims at providing low NOx methodologies to be applied to design these combustors.

References

- [1] J. W. Strutt, Lord Rayleigh, 1878. "The explanation of certain acoustical phenomena". *Notices of the proceedings members of the Royal Institution (of Great Britain)*, **3**, pp. 536–542.
- [2] Crocco, L., and Cheng, S., 1956. *Theory of combustion instability in liquid propellant rocket motors*. AGARDOGRAPH number 8, Butterworths Science Publication.
- [3] Putnam, A., 1971. *Combustion driven oscillations in industry*. Elsevier, New-York.
- [4] Candel, S., Huynh, C., and Poinso, T., 1996. *Unsteady Combustion*. Kluwer Academic Publishers, ch. 5. Some modeling methods of combustion instabilities, pp. 83–112.
- [5] Culick, F. E. C., 2001. *Dynamics of combustion systems : fundamentals, acoustics and control*. NASA.
- [6] Candel, S., 2002. "Combustion dynamics and control: progress and challenges". *Proc. Combust. Inst.*, **29**, pp. 1–28.
- [7] Lieuwen, T., 2005. "Nonlinear kinematic response of premixed flames to harmonic velocity disturbances". *Proc. Combust. Inst.*, **30**, pp. 1725–1732.
- [8] Huang, Y., and Yang, V., 2009. "Dynamics and stability of lean-premixed swirl-stabilized combustion". *Prog. Energy Combust. Sci.*, **35**(4), pp. 293 – 364.
- [9] Paschereit, C., Schuermans, B., Polifke, W., and Mattson, O., 2002. "Measurement of transfer matrices and source terms of premixed flames". *J. Eng. Gas Turbines and Power*, **124**(2), pp. 239–247.
- [10] Krebs, W., Flohr, P., Prade, B., and Hoffmann, S., 2002. "Thermoacoustic stability chart for high-intensity gas turbine combustion systems". *Combust. Sci. Tech.*, **174**(7), pp. 99–128.
- [11] Dowling, A., and Stow, S., 2003. "Acoustic analysis of gas turbine combustors". *J. Propul. Power*, **19**(5), Sep-Oct, pp. 751–764.
- [12] Noiray, N., Durox, D., Schuller, T., and Candel, S., 2006. "Self-induced instabilities of premixed flames in a multiple injection configuration". *Combust. Flame*, **145**(3), pp. 435–446.
- [13] Truffin, K., and Poinso, T., 2005. "Comparison and extension of methods for acoustic identification of burners". *Combust. Flame*, **142**(4), pp. 388–400.
- [14] Kim, K., Lee, J., Lee, H., Quay, B., and Santavicca, D., 2010. "Characterization of forced flame response of swirl-stabilized turbulent lean-premixed flames in a gas turbine combustor". *J. Eng. Gas Turbines and Power*, **132**(4), p. 041502.
- [15] Durox, D., Schuller, T., Noiray, N., and Candel, S., 2009. "Experimental analysis of nonlinear flame transfer functions for different flame geometries". *Proc. Combust. Inst.*, **32**, pp. 1391–1398.

- [16] Karimi, N., Brear, M., Jin, S., and Monty, J., 2009. "Linear and non-linear forced response of a conical, ducted, laminar premixed flame". *Combust. Flame*, **156**(11), pp. 2201 – 2212.
- [17] Dowling, A., 1999. "A kinematic model of a ducted flame". *J. Fluid Mech.*, **394**(1), pp. 51–72.
- [18] Balachandran, R., Ayoola, B., Kaminski, C., Dowling, A., and Mastorakos, E., 2005. "Experimental investigation of the non linear response of turbulent premixed flames to imposed inlet velocity oscillations". *Combust. Flame*, **143**(1-2), pp. 37–55.
- [19] Bellows, B., Bobba, M., Forte, A., Seitzman, J., and Lieuwen, T., 2007. "Flame transfer function saturation mechanisms in a swirl-stabilized combustor". *Proc. Combust. Inst.*, **31**, pp. 3181–3188.
- [20] Kim, D., Lee, J., Quay, B., Santavicca, D., Kim, K., and Srinivasan, S., 2010. "Effect of flame structure on the flame transfer function in a premixed gas turbine combustor". *J. Eng. Gas Turbines and Power*, **132**(2), p. 021502.
- [21] Bellows, B., Zhang, Q., Neumeier, Y., Lieuwen, T., and Zinn, B., 2003. "Forced response studies of a premixed flame to flow disturbances in a gas turbine forced response studies of a premixed flame to flow disturbances in a gas turbine combustor". In 41st AIAA Aerospace Sciences Meeting, AIAA-2003-0824, AIAA, ed., Vol. 824.
- [22] Noiray, N., Durox, D., Schuller, T., and Candel, S., 2008. "A unified framework for nonlinear combustion instability analysis based on the flame describing function". *J. Fluid Mech.*, **615**, pp. 139–167.
- [23] Hurlle, I., Price, R., Sudgen, T., and Thomas, A., 1968. "Sound emission from open turbulent premixed flames". *Proc. R. Soc. London, Ser. A*, **303**, pp. 409–427.
- [24] Higgins, B., McQuay, M., Lacas, F., Rolon, J., Darabiha, N., and Candel, S., 2001. "Systematic measurements of oh chemiluminescence for fuel-lean, high-pressure, premixed, laminar flames". *Fuel*, **80**(1), pp. 67 – 74.
- [25] Noiray, N., Durox, D., Schuller, T., and Candel, S., 2009. "A method for estimating the noise level of unstable combustion based on the flame describing function". *Int. J. Aeroacoustics*, **8**(1), pp. 157–176.
- [26] Poinot, T., Trouve, A., Veynante, D., Candel, S., and Esposito, E., 1987. "Vortex-driven acoustically coupled combustion instabilities". *J. Fluid Mech.*, **177**(1), pp. 265–292.
- [27] Poinot, T., and Veynante, D., 2001. *Theoretical and Numerical Combustion*. Edwards, Philadelphia.
- [28] Culick, F. E. C., 2006. *Unsteady motions in combustion chambers for propulsion systems*. AGARDograph, NATO/RTO-AG-AVT-039.
- [29] Melling, T. H., 1973. "The acoustic impedance of perforates at medium and high sound pressure levels". *J. Sound Vib.*, **29**(1), pp. 1–65.
- [30] Schuller, T., Durox, D., and Candel, S., 2003. "A unified model for the prediction of laminar flame transfer functions : comparisons between conical and v-flame dynamics". *Combust. Flame*, **134**, pp. 21–34.
- [31] Kornilov, V., Rook, R., ten Thije Boonkkamp, J., and de Goey, L., 2009. "Experimental and numerical investigation of the acoustic response of multi-slit bunsen burners". *Combust. Flame*, **156**(10), pp. 1957 – 1970.
- [32] Durox, D., Schuller, T., Noiray, N., Birbaud, A., and Candel, S., 2009. "Rayleigh criterion and acoustic energy balance in unconfined self-sustained oscillating flames". *Combust. Flame*, **156**, pp. 106–119.